KSME

Springer

Journal of Mechanical Science and Technology 37 (7) 2023

Original Article
DOI 10.1007/s12206-023-0625-0

Keywords:
· Titanium alloy
· Strain hardening
· Inverse method
· Deformation
· Tension test

Correspondence to:
Hao Zhang
hao.zhang@yzu.edu.cn

Citation:
Zhang, H., Xu, C., Gao, T., Li, X., Song, H. (2023). Identification of strain hardening behaviors in titanium alloys using tension tests and inverse finite element method. Journal of Mechanical Science and Technology 37 (7) (2023) 3593~3599. http://doi.org/10.1007/s12206-023-0625-0

Received October 23rd, 2022
Revised February 12th, 2023
Accepted March 8th, 2023

† Recommended by Editor Hyun-Gyu Kim

Identification of strain hardening behaviors in titanium alloys using tension tests and inverse finite element method

Hao Zhang[1], Chang Xu[1], Tao Gao[1], Xunpeng Li[1] and Haipeng Song[2]

[1]School of Mechanical Engineering, Yangzhou University, Yangzhou 225127, China, [2] Sino-European Institute of Aviation Engineering, Civil Aviation University of China, Tianjin 300300, China

Abstract This study proposes an inverse methodology for determining the strain hardening behaviors at large deformation of titanium alloys using uniaxial tensile and notched tests with finite element analysis. Various hardening laws and data fitting range are considered to characterize the stress-strain relationships of commercially pure titanium (CP-Ti) and Ti6Al4V alloys which can increase the flexibility of identifying the proper models. A new hybrid HHSL hardening model is presented for CP-Ti and its parameters are obtained by iteratively minimizing the difference between the finite element simulation and experimental data. The hardening behavior of Ti6Al4V alloy is predicted by the weighted HSV model. The results show that mechanical response and loading curves from the identified numerical models are consistent with the experimental results of titanium alloys, demonstrating the validity and effectiveness of the proposed inverse approach in practical use.

1. Introduction

Titanium and its alloys are widely used in aircraft, chemical and biomedical fields due to their excellent properties of high strength-to-weight ratios, endurance to fatigue, good corrosion resistance and superior biocompatibility [1-3]. Titanium alloy usually consists of hexagonal close-packed (HCP) structured α-phase and body-centered cubic (BCC) structured β-phase, and the hierarchical nanostructures lead to its complex plastic deformation mechanisms [4, 5]. Therefore, it is of great significance to further study the elastoplastic deformation behaviors of titanium alloys.

True stress-strain relationships obtained from experiments are often used to identify hardening models of ductile materials by fitting the pre-necking stress-strain data of standard uniaxial tensile test, and then it is extrapolated to the large strain range [6-8]. Accurate material properties and stress-strain relationship are important for the reliable numerical analysis of plastic deformation process with large strains [9, 10]. Zhao et al. obtained the flow curve of sheet metals by iterative extrapolation in the post-necking regime using tensile test and finite element analysis [11]. Reis et al. proposed an inverse methodology for determining the work hardening Swift law parameters by using the results of pole height and pressure from the bulge test [12]. Different hardening laws have great influence on description of the stress-strain relationship at large strains. Kweon et al. used the information at the necking and the fracture points from the tensile test to conduct finite element analysis iteratively and adjust the exponent n of Hockett-Sherby hardening model to determine the true stress-strain equation [13]. The use of combined hardening models consisting a mixture of hardening laws can effectively increase the flexibility of model [14-16]. Barnwal et al. obtained the hardening parameters of mixed Swift and Voce law for DP980 steel by uniaxial tensile and shear tests simulations [17]. Yu et al. conducted an inverse analysis to determine the weighting factor of the mixed Swift and Voce model for L907A steel [18].

Considering the effects of temperature, the H/V model is used to describe the transition of the

strain hardening behavior from the power-type to the saturation-type at low and high temperatures of dual-phase steels [19, 20]. Guo et al. developed a extrapolation constitutive model of titanium alloy sheet under hot-working condition which described the flow behaviors at large deformation [21]. Razali et al. described the flow stress as a set of piecewise bi-linear and closed-form functions to describe the plastic deformation of metals and alloys at different strain rates and elevated temperatures [22]. Li et al. used a mixed Swift-Voce type hardening model coupled with strain rate and temperature-dependent terms to identify the deformation and ductile fracture behaviors of L907A ship steel [23]. The DIC method has become an important tool to obtain the hardening behavior of materials in recent years [24-26]. Zhu et al. measured the shape and deformation of cylindrical specimens by DIC and determined the true stress-strain curves of low carbon steel [27]. Paul et al. corrected the local stress and strain at the diffuse necking region by using the Hill's anisotropic yield criteria and local strains measured by DIC technique [28]. Mu et al. used three parabolic functions to simplify the diffusion necking deformation and established a hardening model to solve the uniaxial tensile true stress and strain in the diffusion necking by 3D-DIC and finite element simulation [29]. The area of the necking sections of AA6061-T6 and AA7075-T6 tensile specimens is estimated, and the weld joint's post necking behavior is predicted by full field strain measurement [30]. However, due to the highly localized and large deformation after necking, it is still a challenge to identify accurately the strain hardening behaviors of titanium alloys.

In this study, the uniaxial and notched tensile tests are conducted on commercially pure titanium (CP-Ti) and Ti6Al4V alloys under large plastic deformation. The stress-strain curves are calculated from the uniaxial tensile specimens and fitted with different strain hardening laws. Hybrid hardening models are proposed to characterize the plastic behaviors of the titanium alloys. An inverse identification method is presented to obtain the most fitting strain hardening model by using experimental and finite element analysis. The difference between the hardening curves obtained by the inverse method and experimental data is evaluated to identify the better hardening models for the CP-Ti and Ti6Al4V alloys.

2. Experiment

The test materials in this work are CP-Ti and Ti6Al4V alloy with the thicknesses of 1 and 0.6 mm, respectively. The uniaxial and notched (R = 5 mm) tensile specimens were fabricated by wire electro discharge machining in rolling direction of the sheets. The dimensions of test specimens are illustrated in Fig. 1. The test samples were loaded until failure on a 5 kN Deben Microtest machine at room temperature. For uniaxial tensile tests, the load speed is 0.6 mm/min which is at a strain rate of 10^{-3}/s until fracture. The crosshead velocity is 0.3 mm/min for notched tension samples.

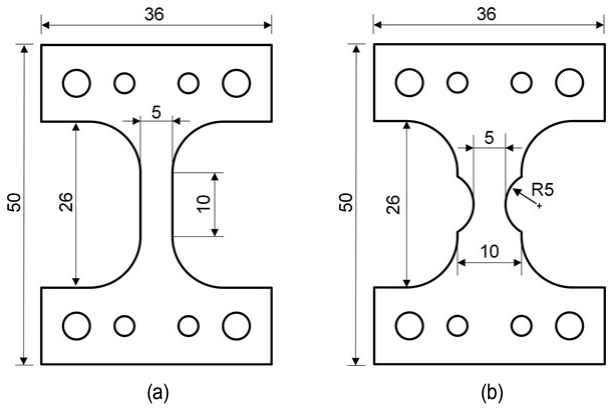

Fig. 1. The dimensions of test specimens: (a) uniaxial tensile; (b) notched tensile (R = 5 mm).

3. Methodology

The main aim of this study is to identify the appropriate strain hardening laws for the titanium alloys. The uniaxial and notched tensile experimental data were used to identify the parameters of constitutive models. The true stress-strain curve of uniaxial tensile specimen before necking can be obtained by

$$\sigma_{\text{true}} = \sigma_{\text{eng}}\left(1+\varepsilon_{\text{eng}}\right) \tag{1}$$

$$\varepsilon_{\text{true}} = \ln\left(1+\varepsilon_{\text{eng}}\right) \tag{2}$$

where σ_{true} and $\varepsilon_{\text{true}}$ are the true stress and strain, respectively; σ_{eng} and ε_{eng} are the engineering stress and strain.

After necking, some physical phenomena such as the local plastic instability, rapid damage accumulation and cross-sectional shape reduction may cause significant errors, which makes the Eqs. (1) and (2) no longer valid theoretically. Therefore, several hardening models have been proposed to describe the true stress-strain relationship after necking, as shown in Table 1. The σ, ε are the true stress and plastic strain where the P_1, P_2, P_3 and P_4 are the parameters. Fitting different hardening models with the pre-necking curves can determine the model's parameters. But the direct extrapolation of the hardening model is usually not accurate due to the complex stress state in the localized necking zone of the testing specimen.

The strategy for identifying the strain hardening model of titanium alloys is shown in Fig. 2. The uniaxial tensile tests are conducted to construct the engineering stress and strain curves. Several strain hardening models are fitted with the pre-necking true stress-strain data to obtain the initial values of their parameters. These models are used in finite element simulation of uniaxial tensile tests to obtain the numerical results of stress-strain curves. The difference between the simulated and experimental stresses is calculated according to $\Delta_1 = \frac{1}{n}\sum_{i=1}^{n}\left|\frac{\sigma_{Eng}^{Num}-\sigma_{Eng}^{Exp}}{\sigma_{Eng}^{Exp}}\right|$ and compared with a predefined toler-

Table 1. Several hardening models and their formulations.

Model	Formulation	
Ludwik (1909) [31]	$\sigma = P_1 + P_2 \cdot \varepsilon^{P_3}$	(3)
Swift (1952) [32]	$\sigma = P_1 \cdot (P_2 + \varepsilon)^{P_3}$	(4)
Ludwigson (1971) [33]	$\sigma = P_1 \cdot \varepsilon^{P_2} + \exp(P_3 + P_4 \cdot \varepsilon)$	(5)
Voce (1948) [34]	$\sigma = P_1 + P_2 \cdot [1 - \exp(-P_3 \cdot \varepsilon)]$	(6)
Hockett and Sherby (1975) [35]	$\sigma = P_1 + P_2 \cdot [1 - \exp(-P_3 \cdot \varepsilon^{P_4})]$	(7)

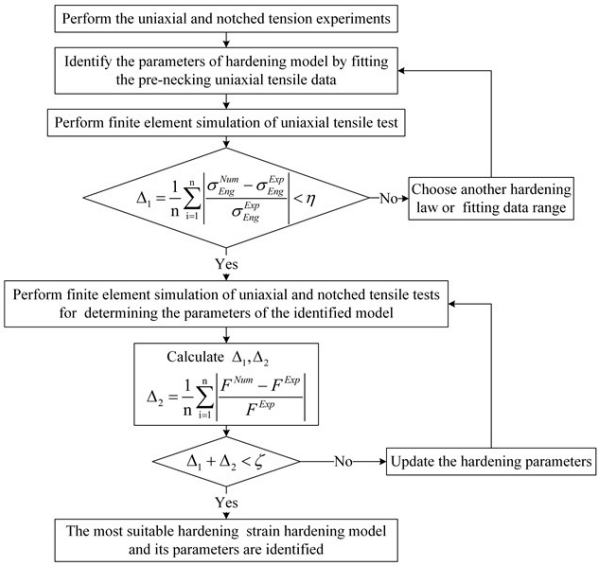

Fig. 2. Strategy for identifying the strain hardening parameters of titanium alloys.

ance η. If Δ_1 is less than tolerance η, the hardening model is identified. Otherwise, another hardening model will be chosen to perform the fitting process until the expression $\Delta_1 < \eta$ is satisfied. Next, the identified model is used in finite element simulation of notched tensile specimens. The difference between the simulated and experimental forces is calculated by $\Delta_2 = \frac{1}{n}\sum_{i=1}^{n}\left|\frac{F^{Num} - F^{Exp}}{F^{Exp}}\right|$. The strain hardening parameters are optimized by minimizing the difference between the experiment and the numerical simulation results in uniaxial tensile and notched tests. The hardening parameters are updated until the $\Delta_1 + \Delta_2 < \zeta$. Thus, the most suitable hardening model and its parameters are identified.

4. Results and discussion

4.1 Uniaxial tensile test

The typical engineering stress-strain curves of uniaxial tensile specimens of CP-Ti and Ti6Al4V alloy are shown in Fig. 3. The Young's modulus E, yield stress σ_y, ultimate tensile stress σ_u and strain at failure ε_f are listed in Table 2. At the initial loading stage, the deformation of the specimen is very small and the stress increases linearly in Fig. 3. The Young's modulus of Ti6Al4V has a little difference with CP-Ti, while the yield stress and ultimate tensile stress of Ti6Al4V are much higher than CP-Ti. The strain at failure of CP-Ti is larger indicating the better ductility than Ti6Al4V alloy.

Table 2. Mechanical properties of titanium alloys.

Material	E (GPa)	σ_y (MPa)	σ_u (MPa)	ε_f
CP-Ti	108.6	315	347	0.52
Ti6Al4V	124.2	1134	1111	0.21

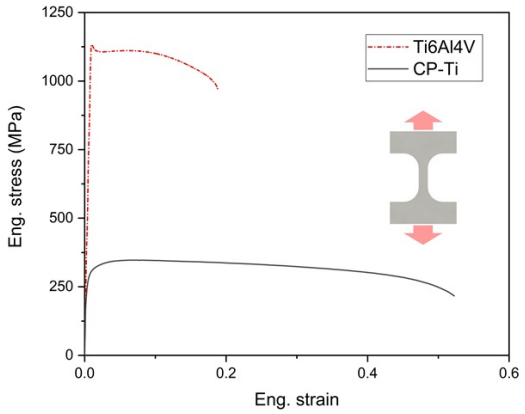

Fig. 3. Engineering stress-strain curves of CP-Ti and Ti6Al4V alloy in uniaxial tensile tests.

4.2 Inverse identification of the strain hardening model

The strategy proposed in Fig. 2 is used to identify the strain hardening behaviors of CP-Ti. Numerical simulations for tensile tests are performed using finite element software Abaqus/Explicit. Fig. 4 shows the mesh and boundary condition of 3D full size finite element (FE) model for uniaxial tensile test. The specimen is discretized by 8-node linear reduced-integration solid elements (C3D8R) with 5 layers through the thickness. The element size is approximately 0.2 mm in the central gauge region and larger at sections away from this area. Upper end of the specimen model is fixed and the other end is subjected to displacement boundary condition. The force F^{Num} is acquired from the bottom edge of the specimen and the engineering stress can be calculated by $\sigma_{Eng}^{Num} = F^{Num}/A_0$, A_0 is initial cross-sectional area. The elongation δl in gauge length can be obtained by the relative displacement between the points N_1 and N_2 which are at the boundary of the gauge length. the engineering strain is calculated by $\varepsilon_{Eng}^{Num} = \delta l/l_0$, l_0 is gauge length 10 mm.

Five hardening models in Table 1 are fitted with the full true stress and plastic strain data in the pre-necking regime of the uniaxial tensile tests. The parameters of the models are de-

termined by the least square method and the results are plotted in Fig. 5(a). The five hardening models are consistent with the experimental data in pre-necking regime while significant deference of these models can be seen after necking. The stresses of Voce and Hockett-Sherby hardening laws saturate into a constant value with plastic strain whereas other curves continue to increase gradually. The simulation results of engineering stress-strain curve are presented in Fig. 5(b). The five different hardening laws which are fitted the full pre-necking data obviously underestimate the strain hardening behavior of CP-Ti after the necking at large deformation.

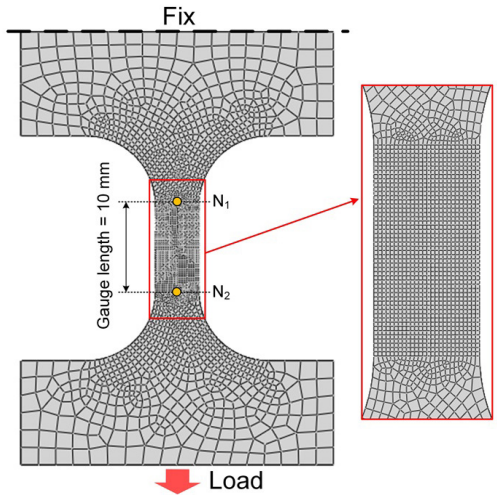

Fig. 4. Mesh and boundary conditions of FE model for the uniaxial tensile tests. The orange points N_1 and N_2 highlight the position of the virtual extensometers for the measurement of relative displacement.

The last half of the experimental data are also used for fitting with the five hardening models, the results are shown in Figs. 5(c) and (d). Before the necking point, the five models obviously overestimate the strain hardening behavior of CP-Ti. Considering the distinct difference between the predicted and experimental results before and after the necking, it is hard to characterize the whole deformation process of CP-Ti accurately by using a single model.

A hybrid strain hardening model, hybrid Hockett-Sherby and Ludwik (HHSL), is proposed to describe the strain hardening behavior of CP-Ti as follows:

$$\sigma_{\text{true}} = \begin{cases} P_1 + P_2 \cdot \left[1 - \exp\left(-P_3 \cdot \varepsilon^{P_4}\right)\right], \varepsilon \le \varepsilon_{\max} \\ P_5 + P_6 \cdot \varepsilon^{P_7}, \varepsilon > \varepsilon_{\max} \end{cases} \tag{8}$$

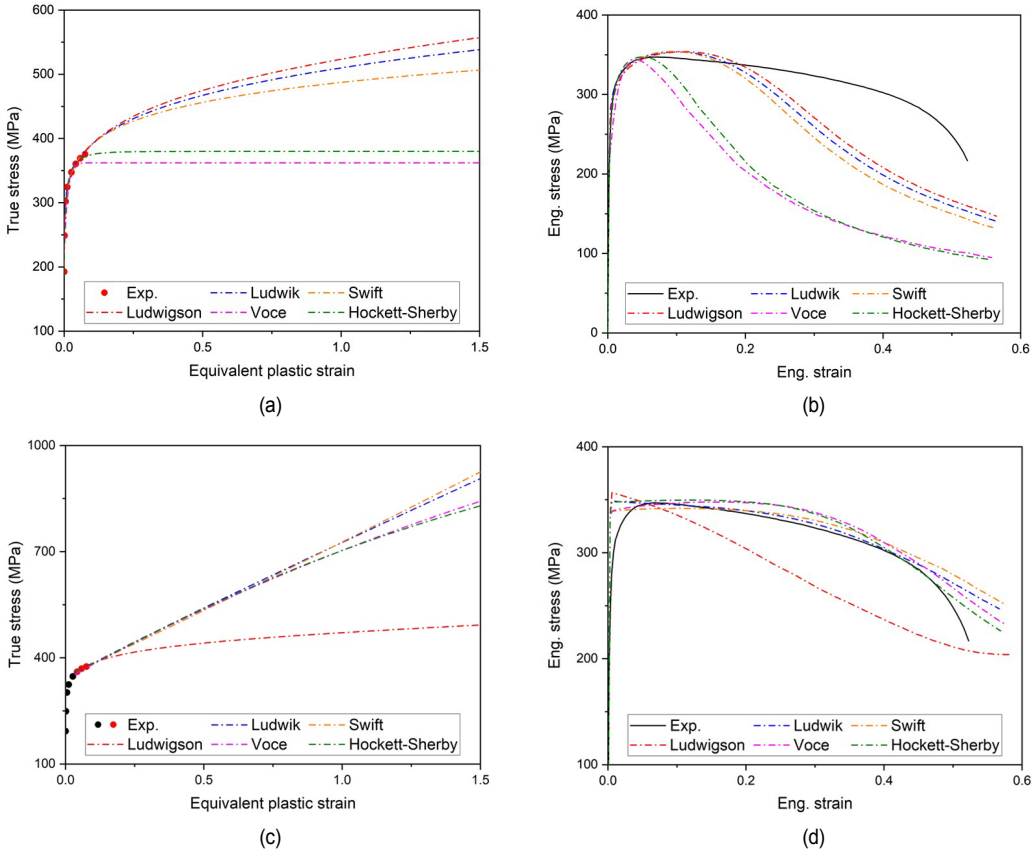

Fig. 5. Comparison between experimental and numerical data for (a) true stress- plastic strain; (b) engineering stress-strain curves fitted with the full experimental data; (c) true stress- plastic strain; (d) engineering stress-strain curves fitted with the last 1/2 experimental data (CP-Ti, uniaxial tension). The experimental data used for fitting are marked as red dots.

Table 3. The identified parameters of hardening model for CP-Ti.

Model	P_1	P_2	P_3	P_4	P_5	P_6	P_7
HHSL	205	158	30	0.7	345	370	1.04

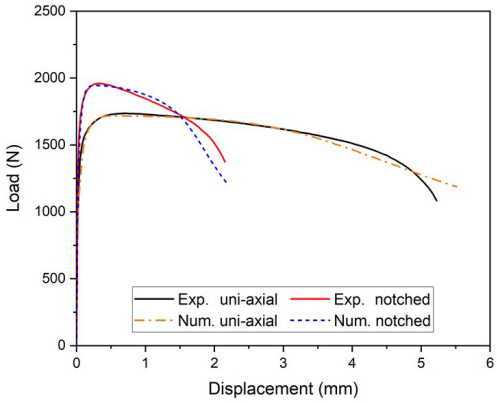

Fig. 6. Comparison of the loading curves of CP-Ti measured from experiment and predicted by the HHSL model.

where $\sigma_{\text{true}} = P_1 + P_2 \cdot \left[1 - \exp\left(-P_3 \cdot \varepsilon^{P_4}\right)\right]$ is the formula of the Hockett-Sherby model applied in the pre-necking region, and $\sigma_{\text{true}} = P_5 + P_6 \cdot \varepsilon^{P_7}$ is the formula of the Ludwik model applied in the post-necking region. P_1, P_2, P_3 and P_4 are the coefficients of the Hockett-Sherby model, while P_5, P_6 and P_7 are the parameters of the Ludwik model. $\varepsilon_{\max}$ is the strain at the onset of necking.

The identified parameters of the HHSL model are listed in Table 3, and the corresponding results of uniaxial and notched (R = 5 mm) tensile specimens are shown in Fig. 6. It can be seen that the numerical predicted curves are consistent with the experimental result.

A non-linear isotropic hardening model is employed to characterize the hardening behaviors of cold-rolled Ti6Al4V alloy. It is combined of hybrid Swift and Voce laws with a weighting factor w, HSV model namely, expressed as:

$$\sigma = w \cdot \sigma_S + (1 - w)\sigma_V \tag{9}$$

where $\sigma_S = P_1 \cdot (P_2 + \varepsilon)^{P_3}$, $\sigma_V = P_4 + P_5 \cdot \left[1 - \exp\left(-P_6 \cdot \varepsilon\right)\right]$ are the Swift and Voce hardening laws, P_1, P_2 and P_3 are coefficients of the Swift model, P_4, P_5 and P_6 are the parameters of Voce model, w is a weighting factor which is in the range of $0 \le w \le 1$.

The uniaxial and notched tensile tests are performed on Ti6Al4V alloy to calibrate the hardening parameters of HSV model and the results are listed in Table 4. The experimental result of uniaxial specimen indicates that the weighting factor w is between 0.6 and 0.7 in Fig. 7(a). A good agreement is observed between the simulation with the weighting factor of 0.5 and the notched tensile results, as shown in Fig. 7(b). Identification of hardening behaviors on Ti6Al4V alloy validates the effectiveness and flexibility of the proposed method.

Table 4. Hardening model parameters for Ti6Al4V alloy.

Model	P_1	P_2	P_3	P_4	P_5	P_6
HSV	301.7	1.9	2.1	1108.6	260.9	6.3

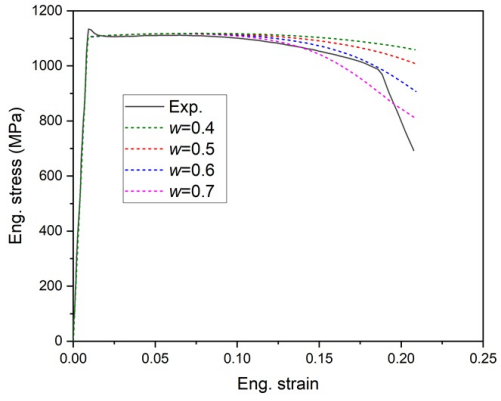

(a)

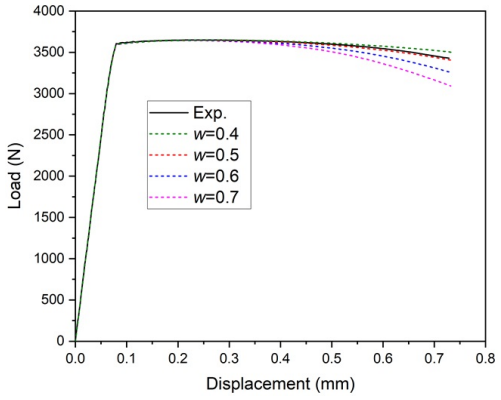

(b)

Fig. 7. Comparison of experimental and numerical results of Ti6Al4V alloy: (a) uniaxial tensile specimen; (b) notched tensile specimen.

5. Conclusions

In the present work, uniaxial and notched tensile tests were conducted to investigate the strain hardening behaviors for CP-Ti and Ti6Al4V alloys. An inverse identification strategy combined curve-fitting and finite element method is proposed to identify the strain hardening model and its parameters. Various hardening laws and different experimental data ranges are considered to fit with the pre-necking true stress-strain curves. The strain hardening model is constructed and parameters are optimized by iteratively minimizing the difference between the finite element simulation results and experimental data from uniaxial tensile and notched tests.

It is found that post necking behaviors of CP-Ti is significantly different from deformation before necking. The piecewise HHSL model is proposed to characterize the hardening

behaviors of CP-Ti in the large deformation region. The finite element simulations incorporated with HHSL model could predict the load-displacement curves of uniaxial and notched tensile specimens with high accuracy.

A weighted hybrid hardening HSV model is used to describe the hardening behavior of Ti6Al4V alloy. The hardening parameters of the HSV model are successfully identified by comparing the simulated loading curves and experimental data of uniaxial and notched tensile specimens. The proposed identification method can effectively identify the hardening behaviors of CP-Ti and Ti6Al4V alloys which show the potential applicability on other ductile materials.

Acknowledgments

This work was supported by the Natural Science Research of Jiangsu Higher Education Institutions of China (Grant No. 21KJB130002) and National Natural Science Foundation of China (Grant No. 11972364).

Nomenclature

σ_{true} : True stress
ε_{true} : True strain
σ_{eng} : Engineering stress
ε_{eng} : Engineering strain
σ : True stress
ε : Plastic strain
P_1 ,…, P_7 : Hardening model parameters
Δ_1 : Difference between the simulated and experimental stresses
σ_{Eng}^{Num} : Simulated stress
σ_{Eng}^{Exp} : Experimental stress
η : Predefined tolerance of difference between the simulated and experimental stresses
Δ_2 : Difference between the simulated and experimental forces
F^{Num} : Simulated force
F^{Exp} : Experimental force
ζ : Predefined tolerance of difference between the simulated and experimental forces
E : Young's modulus
σ_y : Yield stress
σ_u : Ultimate tensile stress
ε_f : Strain at failure
A_0 : Initial cross-sectional area
δl : Elongation in gauge length
l_0 : Gauge length
ε_{max} : Strain at the onset of necking
w : Weighting factor
σ_S : Swift hardening law
σ_V : Voce hardening law

References

[1] E. T. Furton, A. E. Wilson-Heid and A. M. Beese, Effect of stress triaxiality and penny-shaped pores on tensile properties of laser powder bed fusion Ti-6Al-4V, *Addit. Manuf.*, 48 (2021) 102414.

[2] F.-Q. Li, J. Zhao, J.-H. Mo, J.-J. Li and L. Huang, Comparative study of the microstructure of Ti-6Al-4V titanium alloy sheets under quasi-static and high-velocity bulging, *J. Mech. Sci. Technol.*, 31 (3) (2017) 1349-1356.

[3] H. Zhang, X. Li, T. Gao, H. Song and G. Huang, Experimental study on deformation evolution and fracture behaviors of pure titanium at different stress triaxialities, *Eng. Fract. Mech.*, 258 (2021) 108127.

[4] M. Ruiz de Sotto, P. Longère, V. Doquet and J. Papasidero, A constitutive model for a rate and temperature-dependent, plastically anisotropic titanium alloy, *Int. J. Plasticity*, 134 (2020) 102777.

[5] F. R. Kaschel, R. K. Vijayaraghavan, A. Shmeliov, E. K. McCarthy, M. Canavan, P. J. McNally, D. P. Dowling, V. Nicolosi and M. Celikin, Mechanism of stress relaxation and phase transformation in additively manufactured Ti-6Al-4V via in situ high temperature XRD and TEM analyses, *Acta Mater.*, 188 (2020) 720-732.

[6] S. Tu, X. Ren, J. He and Z. Zhang, Stress-strain curves of metallic materials and post-necking strain hardening characterization: A review, *Fatigue Fract. Eng. M.*, 43 (2020) 3-19.

[7] J. Agirre, L. Galdos, E. S. de Argandoña and J. Mendiguren, Hardening prediction of diverse materials using the digital image correlation technique, *Mech. Mater.*, 124 (2018) 71-79.

[8] H. D. Kweon, E. J. Heo, D. H. Lee and J. W. Kim, A methodology for determining the true stress-strain curve of SA-508 low alloy steel from a tensile test with finite element analysis, *J. Mech. Sci. Technol.*, 32 (7) (2018) 3137-3143.

[9] C. Zhang, Y. Lou, S. Zhang, T. Clausmeyer, A. E. Tekkaya, L. Fu, Q. Chen and Q. Zhang, Large strain flow curve identification for sheet metals under complex stress states, *Mech. Mater.*, 161 (2021) 103997.

[10] M. Saboori, H. Champliaud, J. Gholipour, A. Gakwaya, J. Savoie and P. Wanjara, Evaluating the flow stress of aerospace alloys for tube hydroforming process by free expansion testing, *Int. J. Adv. Manuf. Tech.*, 72 (2014) 1275-1286.

[11] K. Zhao, L. Wang, Y. Chang and J. Yan, Identification of post-necking stress-strain curve for sheet metals by inverse method, *Mech. Mater.*, 92 (2016) 107-118.

[12] L. C. Reis, P. A. Prates, M. C. Oliveira, A. D. Santos and J. V. Fernandes, Inverse identification of the Swift law parameters using the bulge test, *Int. J. Mater. Form.*, 10 (2017) 493-513.

[13] H. D. Kweon, J. W. Kim, O. Song and D. Oh, Determination of true stress-strain curve of type 304 and 316 stainless steels using a typical tensile test and finite element analysis, *Nucl. Eng. Technol.*, 53 (2021) 647-656.

[14] Q. T. Pham, T. Nguyen-Thoi, J. Ha and Y.-S. Kim, Hybrid fitting-numerical method for determining strain-hardening behavior of sheet metals, *Mech. Mater.*, 161 (2021) 104031.

[15] P. D. Versaillot, Z.-L. Zhao and Y.-F. Wu, A new theoretical method for predicting the elastoplastic behavior of ductile metallic materials, *Int. J. Mech. Sci.*, 200 (2021) 106450.

[16] T. Fras, C. C. Roth and D. Mohr, Fracture of high-strength armor steel under impact loading, *Int. J. Impact Eng.*, 111 (2018) 147-164.
[17] V. K. Barnwal, S.-Y. Lee, J.-H. Kim and F. Barlat, Failure characteristics of advanced high strength steels at macro and micro scales, *Mater. Sci. Eng. A*, 754 (2019) 411-427.
[18] R. Yu, X. Li, Z. Yue, A. Li, Z. Zhao, X. Wang, H. Zhou and T. J. Lu, Stress state sensitivity for plastic flow and ductile fracture of L907A low-alloy marine steel: from tension to shear, *Mater. Sci. Eng. A*, 835 (2022) 142689.
[19] J. H. Sung, J. H. Kim and R. H. Wagoner, A plastic constitutive equation incorporating strain, strain-rate, and temperature, *Int. J. Plasticity*, 26 (2010) 1746-1771.
[20] J. Wang, W.-G. Guo, X. Gao and J. Su, The third-type of strain aging and the constitutive modeling of a Q235B steel over a wide range of temperatures and strain rates, *Int. J. Plasticity*, 65 (2015) 85-107.
[21] J. Guo, M. Zhan, M. W. Fu, P. F. Gao and F. Ma, Extrapolation based constitutive modeling of flow stress of titanium alloy sheet under hot-working condition, *Mater. Design*, 154 (2018) 96-107.
[22] M. K. Razali, M. Irani and M. Joun, General modeling of flow stress curves of alloys at elevated temperatures using bilinearly interpolated or closed-form functions for material parameters, *J. Mater. Res. Technol.*, 8 (2019) 2710-2720.
[23] X. Li, R. Yu, P. Wang, R. Kang, Z. Shu, Z. Yue, Z. Zhao, X. Wang and T. J. Lu, Plastic deformation and ductile fracture of L907A ship steel at increasing strain rate and temperature, *Int. J. Impact Eng.*, 174 (2023) 104515.
[24] J. Li, G. Yang, T. Siebert, M. F. Shi and L. Yang, A method of the direct measurement of the true stress-strain curve over a large strain range using multi-camera digital image correlation, *Opt. Laser. Eng.*, 107 (2018) 194-201.
[25] J. Peirs, P. Verleysen, W. Van Paepegem and J. Degrieck, Determining the stress-strain behaviour at large strains from high strain rate tensile and shear experiments, *Int. J. Impact Eng.*, 38 (2011) 406-415.
[26] H. Zhang, S. Coppieters, C. Jiménez-Peña and D. Debruyne, Inverse identification of the post-necking work hardening behaviour of thick HSS through full-field strain measurements during diffuse necking, *Mech. Mater.*, 129 (2019) 361-374.
[27] F. Zhu, P. Bai, J. Zhang, D. Lei and X. He, Measurement of true stress-strain curves and evolution of plastic zone of low carbon steel under uniaxial tension using digital image correlation, *Opt. Laser. Eng.*, 65 (2015) 81-88.
[28] S. K. Paul, S. Roy, S. Sivaprasad, H. N. Bar and S. Tarafder, Identification of post-necking tensile stress-strain behavior of steel sheet: an experimental investigation using digital image correlation technique, *J. Mater. Eng. Perform.*, 27 (2018) 5736-5743.
[29] Z. Mu, J. Zhao, G. Yu, X. Huang, Q. Meng and R. Zhai, Hardening model of anisotropic sheet metal during the diffuse instability necking stage of uniaxial tension, *Thin-Wall. Struct.*, 159 (2021) 107198.
[30] H. Suthar, A. Bhattacharya and S. K. Paul, DIC-based approach to predict post necking behavior for AA6061, AA7075 and their friction stir welded joints, *Mech. Mater.*, 172 (2022) 104364.
[31] P. Ludwik, *Elemente der Technologischen Mechanik*, Springer Berlin Heidelberg (1909).
[32] H. W. Swift, Plastic instability under plane stress, *J. Mech. Phys. Solids*, 1 (1952) 1-18.
[33] D. C. Ludwigson, Modified stress-strain relation for FCC metals and alloys, *Metall. Trans.*, 2 (1971) 2825-2828.
[34] E. Voce, The relationship between stress and strain for homogeneous deformation, *J. Inst. Metals*, 74 (1948) 537-562.
[35] J. E. Hockett and O. D. Sherby, Large strain deformation of polycrystalline metals at low homologous temperatures, *J. Mech. Phys. Solids*, 23 (1975) 87-98.

Hao Zhang received his Ph.D. from Tianjin University, China, in 2014. Currently, he is a Lecturer in School of Mechanical Engineering, Yangzhou University. His research interests include materials characterization, additive manufacturing, finite element modeling and simulation.